Desalination and Water Treatment
www.deswater.com

doi: 10.5004/dwt.2018.21775

101 (2018) 313–324
January

Efficient adsorption of malachite green dye using *Artocarpus odoratissimus* leaves with artificial neural network modelling

Nur Afiqah Hazirah Mohamad Zaidi, Linda Biaw Leng Lim*, Anwar Usman, Muhammad Raziq Rahimi Kooh

Department of Chemistry, Faculty of Science, Universiti Brunei Darussalam, Jalan Tungku Link, Gadong, Bandar Seri Begawan, BE 1410, Negara Brunei Darussalam, emails: linda.lim@ubd.edu.bn (L.B.L. Lim), afhazirah@gmail.com (N.A.H.M. Zaidi), anwar.usman@ubd.edu.bn (A. Usman), chernyuan@hotmail.com (M.R.R. Kooh)

Received 10 July 2017; Accepted 7 December 2017

ABSTRACT

The utilization of *Artocarpus odoratissimus* (also locally known as *Tarap*) leaves (TL) for the removal of malachite green (MG) dye from simulated wastewater was investigated. We demonstrated that it has a high adsorption efficiency with a maximum adsorption capacity of 254.93 mg g^{-1}. Unlike many reported adsorbents, adsorbent from TL showed little effects upon changes in pH and ionic strength of the medium, supporting their potential to be used in wastewater treatment. The adsorption isotherm of MG by the TL adsorbent was well described by the Redlich–Peterson and Sips isotherm models, and the adsorption kinetics was the pseudo-second order. Thermodynamic quantities of the adsorption process revealed that the adsorption of MG onto TL adsorbent was endothermic, spontaneous, and random. We also showed that the spent TL adsorbent can be well regenerated and reused upon strong base treatment. Artificial neural network model supported the experimental data, and it predicted accurately the effects of some parameters on the adsorption process.

Keywords: *Artocarpus odoratissimus* leaves; Malachite green; Adsorption; Regeneration; Artificial Neural Network Modelling

1. Introduction

Large-scale improvements have been made in industries in order to cater for the rising world population. A direct consequence of the massive industrialization is high consumption of natural resources and excessive wastes, which cause pollutions in air, soil, and water. In the past few decades, the existences of pollutants in water bodies such as groundwater, rivers, lakes, and oceans have become a major problem. Most of it is related to wastewater effluents containing various kinds of synthetic dyes from textile, food processing, cosmetic, rubber, and plastic industries that are directly or indirectly discharged into water drainage systems, and they end up in the water bodies [1]. If such pollutants in the water bodies are inadequately treated, it will have severe effects to human, as it could become one of the leading causes of deaths and diseases. Driven by the existences of such hazardous pollutants in the water bodies, particularly in water resources, different physical, chemical, and biological treatments have been developed to remove them. For instance, photocatalytic degradation [2], thermal decomposition [3], ion exchange [4], reverse osmosis [5], and adsorption processes [6] have been reported and widely discussed to be promising methods in removing the pollutants from water.

Among the aforementioned methods, adsorption of dyes onto the adsorbent has gained great attentions due to the potential of various adsorbents and their simple treatments [7–10]. Therefore, a large number of researches have been intensively devoted on finding new efficient adsorbents as alternative means to remove organic and inorganic pollutants

* Corresponding author.

from water. In addition to commercial zeolites [11,12] and activated carbons [13–15], adsorbents obtained from various sources, including agricultural wastes [16,17], fly ash from industries [18], aquatic plants [19–21], vegetable and fruit wastes [22], peat [23–25], resins [26], fungi [27], and many others [28–30] have been demonstrated to be promising and effective alternatives. However, intensive studies have indicated that adsorbents obtained from fruit wastes are more popular due to their low cost and high adsorption capacity [6,31,32].

Artificial neural network (ANN) is one of the mathematical models inspired by the mechanism of a biological neuron, mimicking our brain's neural network when solving problems. Being a robust, non-linear model, it can deal with noisy data and yet achieve reasonable accuracy in its prediction. The ANN model is a supervised learning based on the generalization of the least mean square error algorithm. The applications of ANN are vast and have been used in forecasting of weather [33], stock markets [34], optimization of industrial processes [35] and environmental monitoring [36]. Recent years have seen the emergence of using ANN in water remediation technology, which include the phytoextraction of basic dye using water fern [37], as well as the adsorption of dyes and heavy metals using agricultural wastes and low-cost adsorbents [37–39].

The present work focuses on the feasibility of *Artocarpus odoratissimus* (also locally known as *Tarap*) leaves as an adsorbent. These *Tarap* leaves (abbreviated as TL) have been considered as a sustainable resource of biomass due to their occurrence in huge volume, leaving behind thick layer of organic mass on the landfill [40]. The effectiveness of adsorbents from the *Artocarpus* family to remove dyes from aqueous solution has been demonstrated by several previous studies [41,42]. On the other hand, the use of skin and core of *Artocarpus odoratissimus* fruit has been intensively explored as adsorbents to remove heavy metals and several toxic dyes, including methylene blue, methyl violet, crystal violet, rhodamine B, malachite green (MG), and brilliant green, and most of the removals were found to be high efficiency [43–48]. As an explorative extension of our ongoing study on wastes of *Artocarpus odoratissimus*, TL was chosen and tested for its potential in removing MG which is a hazardous, toxic, and carcinogenic dye from aqueous solution.

The effects of contact time, pH, and anionic strength on the adsorption of the dye onto TL were systematically examined. The adsorption data were applied to six different isotherm models, whereas the kinetics of the adsorption process was assessed by using pseudo-first-order, pseudo-second-order, intraparticle diffusion, and Boyd equations. We also evaluated regeneration of the spent adsorbent by washing it using acid, base, and water. Further, a three-layer ANN model was employed in this study to predict the performance of TL as a low-cost adsorbent for the removal of MG dye. The data obtained from ANN were compared with the data obtained from batch experiments to explore the feasibility of using ANN as a model in adsorption of MG onto TL.

2. Materials and methods

2.1. Preparation of adsorbent particles of TL

TL were collected from their trees and washed thoroughly in large amount of distilled water to remove any surface dirt. The leaves were dried in an oven at 60°C–70°C for 36 h and they were powdered and passed through metallic sieve mesh 355 μm. These particles were then directly used as adsorbents throughout the experiments.

2.2. Chemicals and reagents

MG chloride, hydrochloric acid (HCl), and sodium hydroxide (NaOH) were purchased from Sigma-Aldrich Chemical Co. (Germany), Auburn (Australia), and Merck (Germany), respectively, and they were used without further purification. Different concentrations of MG were prepared by diluting the 1,000 mg L^{-1} MG stock solution. HCl and NaOH were used for pH adjustment of the MG solutions.

2.3. Characterizations

Size distribution of the adsorbent particles was determined from about 100 bright-field images of individual particles, which were obtained using a high performance microscope (Eclipse 50*i*POL, Nikon, Singapore) with 10× magnification objective lens and a halogen lamp light source. Morphological characteristics of the adsorbent particles were analyzed from their microscopic images obtained by Vega XMU Scanning Electron Microscope (SEM). The particles used for SEM imaging were coated with gold by using SPI-MODULE™ Sputter Coater.

Fluorescence images of the adsorbent particles, before and after MG adsorption, were measured using fluorescence microscope (Eclipse 50*i*POL, Nikon) equipped with a high-power mercury lamp (Digital Sight DS-U3, Nikon) as the source of light excitation. Excitation wavelength at 375 nm was selected by band pass filter. The light was directed on the individual particles on the microscope stage, passing through a 40× magnification lens. Fluorescence signals were captured by the same objective lens, passing through dichroic mirror and long pass filter to cut the elastic scattering of the excitation light, and ultimately detected by a CCD camera. In this measurement, the exposure time was 100 ms and analog gain of the images was set at 4.0 times.

The functional groups in the adsorbent particles of TL were evaluated from their vibrational infrared (IR) spectra, which were measured using Fourier transform infrared (FTIR) spectrophotometer (IRPrestige-21, Shimadzu). The IR spectra of TL, before and after adsorption with MG, were analyzed and compared. Considering that there is no chemical reaction between the adsorbent particles with MG, the spectral changes of TL after MG adsorption could be attributed to the interactions between the functional group on the adsorbent particle's surface with MG.

Adsorption of MG was determined from the difference in adsorption of the dye before and after adsorption process. The absorption spectra of MG solutions were measured by a UV–Vis spectrophotometer (UV-1601 PC, Shimadzu) in cuvette cell with 1 cm optical path. The concentration of MG was determined from the absorption spectrum at 618 nm, at which the extinction coefficient of MG in water is 1.49×10^5 L mol^{-1} cm^{-1} [49].

2.4. Important parameters in adsorption process

2.4.1. Contact time

To investigate the optimum contact time, the mixture of the adsorbent particles and MG (100 mg L^{-1}) with ratio of adsorbent dosage to the dye volume being 1:500 (g:mL) was shaken at 250 rpm for 30 min intervals until 4 h or once the equilibrium is reached. Each solution was filtered off and the absorbance of the filtrate was measured by using a UV–Vis spectrophotometer.

2.4.2. Effect of pH of the medium

pH of MG solutions (100 mg L^{-1}) was adjusted to be in the range of 2–10 by adding HCl or NaOH. Into the pre-weighed adsorbent particles with the same mass (50 mg) in conical flasks, different pH dye solutions (25.0 mL) were added. Each mixture was then shaken at its optimum shaking time and the filtrates were measured.

2.4.3. Effect of ionic strength

Effect of ionic strength on adsorption of MG onto TL was evaluated at different concentrations of KNO_3. In this case, 2 M of KNO_3 was diluted to prepare different concentrations of KNO_3 ranging from 0.01 to 1.0 M in 100 mL volumetric flasks. Into each flask, 10.0 mL of MG solutions (1,000 mg L^{-1}) was added and it was topped up by distilled water. 25.0 mL of these solutions were added into conical flasks containing pre-weighed adsorbent particles with the same mass (0.05 g), and the mixtures were shaken thoroughly for its optimum shaking time.

2.5. Isotherm, thermodynamics, and kinetics studies of adsorption of MG onto TL

To evaluate isotherm of the adsorption process, a series of MG solutions with different concentrations from 0 to 1,000 mg L^{-1} was prepared. Each MG solution (25.0 mL) was added into conical flasks containing pre-weighed adsorbent particles with the same mass (0.05 g), and they were mixed thoroughly at its optimized shaking time. The mixtures were then filtered off, the filtrate was collected and its absorbance was measured.

The thermodynamics of the adsorption was studied by evaluating the process at different temperatures (298, 313, 323, 333, and 343 K). In this case, MG (100 and 500 mg L^{-1}) and adsorbent particles (0.05 g) mixtures were prepared, and each mixture was immersed and shook in a temperature-controlled water bath. After their optimum shaking time, the mixtures were filtrated, and the filtrates were subjected to the absorption measurement.

Kinetics of the adsorption was evaluated in the mixtures of the adsorbent particles (0.05 g) and MG (25.0 mL) with two different dye concentrations (100 and 500 mg L^{-1}). The mixtures were shaken until they reached an equilibrium condition, and at each MG concentration the adsorption was measured at a certain interval time (3 or 15 min).

2.6. Regeneration of the adsorbent particles

For the first cycle, the adsorbent (1.0 g) was mixed with MG (500 mg L^{-1}) in 1.0 L conical flask, hence the adsorbent dosage to dye volume ratio at 1 g per 500 mL. The mixture was shook, and after reaching its optimized shaking time the mixture was filtered off. The filtrate was collected for the absorption recording and the adsorbent particles impregnated with dyes were collected, divided into five portions and treated with different desorbing agents. For this purpose, the adsorbent particles were washed with excessive desorbing agents and shook using shaker at 250 rpm for 2 h. The adsorbent particles were then washed with distilled water until they turned colourless. These spent adsorbent particles were then kept in an oven and ready to use for the next adsorption process. The regeneration was carried out for four consecutive adsorption–desorption cycles.

2.7. Definition of the artificial neural network modelling

In this study, the ANN model was built using a data mining software package, Weka version 3.8 [50]. The ANN is a supervised learning method based on the generalization of the least mean square error algorithm and a gradient descent method is used to minimize the mean square difference between the target and actual net output. The classifier used for the model is "Multilayer perceptron" (back propagation). A general ANN model consists of N neurons in the input layer, M neurons in the hidden layer and O neurons in the output layer and can be represented as N-M-O architecture. In this study, the input layer consists of five neurons which are the adsorbent mass, pH, initial dye concentration, temperature, and contact time, while the output layer consists of only one neuron which is the adsorption capacity. The log sig activation function was used in the hidden layers. A total of 256 data were used in this model, where a stratified 10-fold cross-validation method was used for testing and validation. The performance of the ANN model is evaluated by values of the correlation coefficient (R) and root square mean error (RMSE) which were generated by the Weka software. The number of neurons in the hidden layer was optimized and selected based on the lowest value of RMSE and highest correlation coefficient (R).

3. Results and discussion

3.1. Size distribution, surface morphology, and functional groups of the adsorbent particles

Fig. 1(A) shows size distribution of the adsorbent particles before and after impregnated with MG. The particle sizes are within 350 μm with the maximum size distribution being less than 100 μm. Interestingly, the mean particle size tends to be smaller after adsorption process, most probably due to the mechanical stirring while carrying out the experiment. This further indicates that the adsorbent particles of TL are soft and fragile. A SEM image of an adsorbent particle, as shown in Fig. 1(B) for a representative example, demonstrated roughness of its surface. In particular, the image also shows the presence of groves in μm scales on the surface. The groves and uneven surface expose more functional groups on the particle's surface to interact readily with dyes, resulting in better chemical adsorption of the dyes. They can also be considered as an increase in the surface area of the particle, enhancing its physical adsorption. Thus, from their rough surfaces we can expect that the adsorbent particles of TL would have a high adsorption efficiency, as it will be discussed in section 3.4.

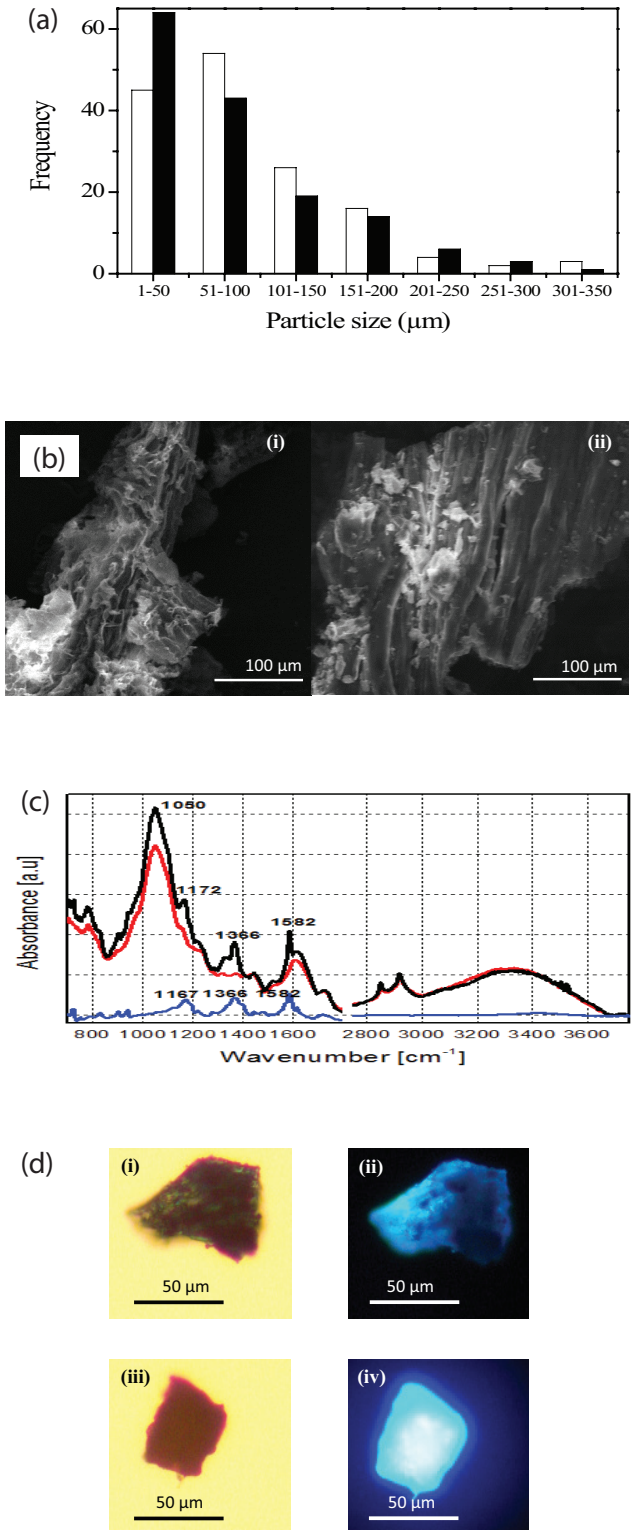

Fig. 1. (A) Particle sizes of TL before (□) and after (■) MG adsorption. (B) SEM images of TL (i) before and (ii) after adsorption of MG. (C) FTIR spectra of TL (— red line), MG (— blue line) and TL-MG (— black line). (D) Images of TL after MG adsorption (i) under bright light (ii) under excitation wavelength of 375 nm while images of (iii) and (iv) are free MG particles under bright light and excitation wavelength, respectively.

Functional groups in the adsorbent particles were evaluated from their IR spectra of the adsorbent particles of TL before and after impregnated with MG, as shown in Fig. 1(C). The IR spectrum of MG is also displayed for comparison. We assigned the vibrational bands of the IR spectra of the TL adsorbent particles as follows: the broad band at 3,350 cm^{-1} to be OH and NH vibrations of hydroxyl and amino groups and sharp bands at 2,850 and 2,900 cm^{-1} to be CH and NH vibrations. The bands in the finger print region at 1,726, 1,611, 1,443, 1,042, and 779 cm^{-1} are assigned to C=O stretching, N–H bending, O–H bending, C–O stretching, and N–H wagging vibration, respectively. This finding indicates that the adsorbent particles have OH, NH_2, CO, and COOH functional groups, which may be involved in the adsorption of MG dyes. Upon adsorption of MG, there are no vibrational changes in the adsorbent particles of TL. Nevertheless, in the IR spectrum of the adsorbent particles impregnated with MG, few additional bands at 1,172, 1,366 and 1,582 cm^{-1} appeared. These new bands are attributable to vibrations of MG, which can be confirmed from the IR spectrum of MG in Fig. 1(C). Therefore, MG dyes are adsorbed by the adsorbent particles of TL through weak interactions rather than via covalent bonds. This provides an interpretation that the chemical structures of both MG and the adsorbent particles remain intact after the adsorption process. Such unchanged structure of MG adsorbed on the adsorbent particles was demonstrated by the same emission of free MG dyes and those adsorbed on the adsorbent particles as shown in Fig. 1(D) for their fluorescence microscopic images.

3.2. ANN modelling

The performance of the ANN prediction of the adsorptive behaviour of MG using TL is summarized in Fig. 2(A). With one neuron in the hidden layer, the ANN model performed reasonably well with correlation coefficient (R) at 0.9413 and RMSE at 0.0744. The performance of the ANN model can be evaluated by both the R^2 and RMSE values, whereby higher R^2 value and lower RMSE value are indicative of better performance of the ANN model. In this study, it was found that the best performance was achieved with four neurons in the hidden layer (R = 0.982, RMSE = 0.418), therefore this was used as the optimum number of neurons in the hidden layer.

The closeness between the experimental data and the ANN predicted data is visualized in Fig. 2(B), which indicated the suitability and reliability of the ANN modelling. The framework and structure of the optimized ANN model used in this study are represented in Fig. 2(C).

3.3. Optimization of contact time and effects of pH and ionic strength

Prior to the adsorption experiments, optimization of time for the adsorbate–adsorbent system to reach equilibrium was investigated. From Fig. 3(A), a rapid increase in dye removal was observed within the first 30 min, attributed to rapid increase in surface coverage of adsorbent by the dye molecules. Under the experimental condition, TL required 3 h of contact time for equilibrium to be reached.

When compared with the untreated (ambient) pH of MG at 3.84, it was observed that apart from a reduction of

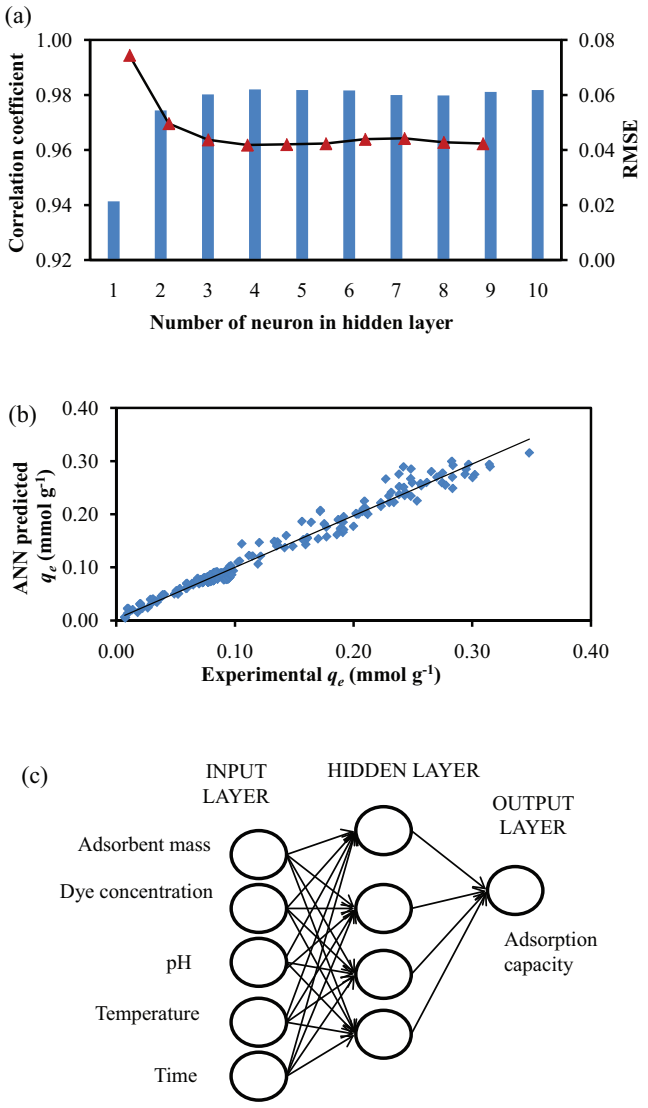

Fig. 2. Graphs showing (A) the correlation coefficient (■) and RMSE (▲) of the number of neurons in the hidden layers, (B) the variation between the ANN predicted data and experimental data with linear line showing correlation coefficient of 0.9763, and (C) the structure of the optimized ANN for modelling adsorption of MG using TL.

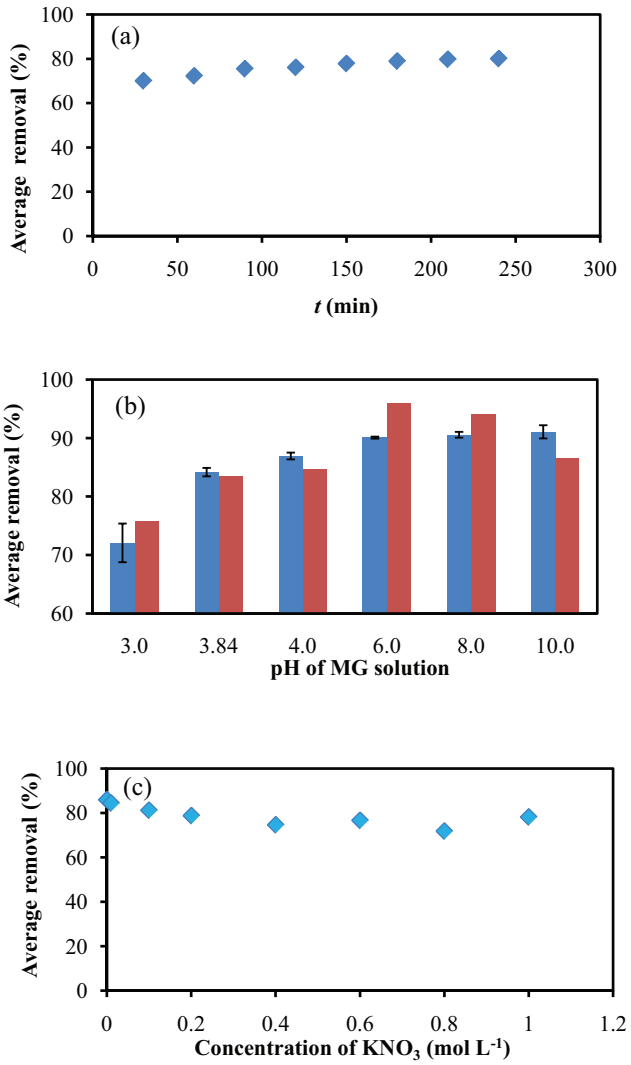

Fig. 3. The effects of (A) contact time, (B) pH with experimental data (■), and ANN predicted (■), and (C) ionic strength using 100 mg L^{-1} MG.

approximately 16% at pH 3 for TL, generally TL is resilient to any changes in the pH of the medium and has the ability to retain their adsorption abilities at different pHs, as shown in Fig. 3(B). Further, the predicted values using the ANN model on the effect of pH on dye adsorption were also reasonably close to the experimental values.

In this study, it was found that TL was able to maintain good adsorption of MG dye (100 mg L^{-1}) at different ionic strengths. As shown in Fig. 3(C), an 8% reduction was observed. For other adsorbents such as breadfruit skin, it was reported to show a 20% reduction in the presence of KNO_3 even at concentration of 0.1 M [51], while breadnut peel and its NaOH modified form [52] showed 17% and 65% reduction, respectively, at the concentration of KNO_3 as low as 0.001 M. Furthermore, many reported adsorbents showed generally highly reduced effectiveness to remove cationic dyes in the presence of salt at various concentrations. For example, *Azolla pinnata* [53] and duckweed [19] were reported to show approximately 40% reduction in the removal of methyl violet dye at 0.9 M and 0.001 M KNO_3, respectively, while cempedak durian peel [54] gave 50% reduction at 0.8 M KNO_3. Hence, short equilibrium contact time coupled with high resilient to both pH and ionic strength pave the way for TL to be a potential adsorbent for the removal of toxic cationic MG dye. It is very important in wastewater treatment that there is a rapid uptake of adsorbate by an adsorbent as this signifies the efficacy of an adsorbent to be used in wastewater treatment and is favourable in terms of cost effectiveness and economical approaches [55].

3.4. Effect of concentration and adsorption isotherm studies

The study of the effect of dye concentration is useful and the data can be fitted into various adsorptive isotherm models

to characterize the adsorption process. The effect of dye concentration is summarized in Fig. 4(A), where the adsorption capacity increases with the dye concentration. This can be explained using the Fick's diffusion law, where higher dye concentration provides more driving force to move the adsorbates onto the adsorbents. It can also be observed that higher temperature resulted in higher adsorption hinting the endothermic nature of the adsorption process. The detailed thermodynamics of the adsorption process is discussed in the section 3.5. The ANN model data showed reasonable accuracy in predicting the effect of dye concentrations as illustrated in Fig. 4(A).

To describe the adsorption process, experimental isotherm data for MG onto TL were fitted to six different isotherm models, namely Langmuir [56], Freundlich [57], Temkin [58], Dubinin–Radushkevich (D–R) [59], Redlich–Peterson (R–P) [60], and Sips [61]. Their non-linear equations are gathered in Table 1. Accuracy of these isothermal models to an adsorption data set was evaluated by four different equation errors (Eqs. (1)–(4)):

$$\text{Average relative error}(\text{ARE}): \frac{100}{n}\sum_{i=1}^{n}\left|\frac{q_{e,\text{meas}}-q_{e,\text{calc}}}{q_{e,\text{meas}}}\right|_i \quad (1)$$

$$\text{Hybrid fractional error function}(\text{HYBRID}): \frac{100}{n-p}\sum_{i=1}^{n}\left[\frac{\left(q_{e,\text{meas}}-q_{e,\text{calc}}\right)^2}{q_{e,\text{meas}}}\right]_i \quad (2)$$

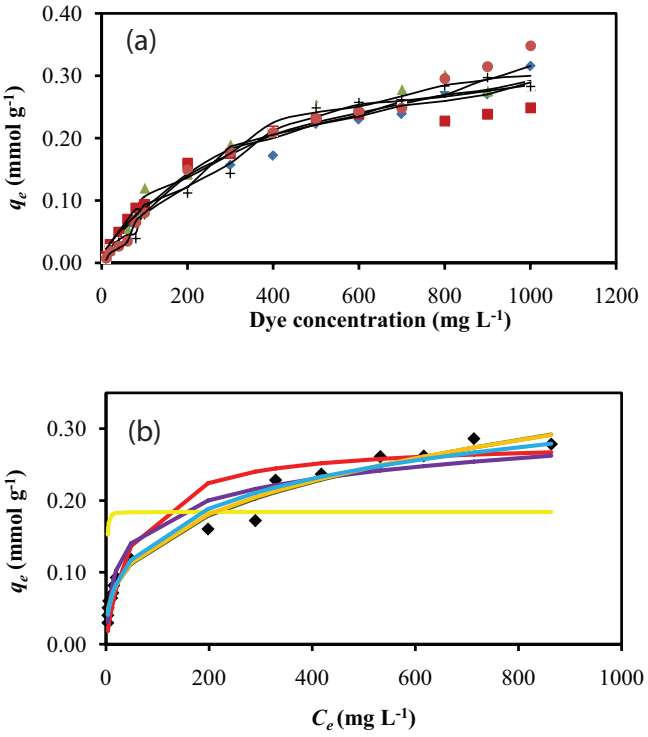

Fig. 4. (A) The effect of dye concentrations on the removal of MG using TL under different temperatures of 298 K (♦), 313 K (▲), 323 K (■), 333 K (+), and 343 K (●) with predicted ANN (—) and (B) simulation plots of different isotherm models of Langmuir (—), Freundlich (—), Temkin (—), D–R (—), R–P (—), and Sips (—) with experimental data (♦).

$$\text{Sum of absolute error}(\text{EABS}): \sum_{i=1}^{n}\left|q_{e,\text{meas}}-q_{e,\text{calc}}\right| \quad (3)$$

Marquardt's percent standard deviation (MPSD):

$$\sqrt[100]{\frac{1}{n-p}\sum_{i=1}^{n}\left(\frac{q_{e,\text{meas}}-q_{e,\text{calc}}}{q_{e,\text{meas}}}\right)_i^2} \quad (4)$$

Here, $q_{e,\text{meas}}$ is the amount of dye adsorbed experimentally, $q_{e,\text{calc}}$ is the calculated adsorbed dye, n is the number of parameters, and p is the number of data points. The main purpose of the inclusion of these equation errors is to reinforce the suitability of the isotherm models to describe the adsorption process.

From the fitting, the D–R isotherm model deviated greatly from the experimental data, as shown in the simulation plots in Fig. 4(B). This is further confirmed by its high overall error values (Table 2). We may note that although the Langmuir isotherm model gave reasonably good R^2 values > 0.94, it has high error values and its simulation plot also deviated from the experimental data. Hence it is also deemed unsuitable. This was followed by Temkin and Freundlich isotherm models. On the other hand, Sips and R–P isotherms are the two best models to describe the adsorption of MG onto TL, where both have comparable overall error values and simulation plots. We may note that Langmuir, Temkin, Freundlich, and D–R isotherm models have two parameters, whereas both Sips and R–P models

Table 1
Non-linear equations of six different isotherm models

Isotherm model	Non-linear equation
Langmuir	$q_e = \frac{q_m k_L C_e}{1+k_L C_e}$
Freundlich	$q_e = K_F C_e^{1/n}$
Temkin	$q_e = \frac{RT\ln\left(k_T C_e\right)}{b_T}$
D–R	$q_e = q_m \exp\left(-\beta\left[RT\ln\left(1+\frac{1}{C_e}\right)\right]^2\right)$
R–P	$q_e = \frac{k_R C_e}{1+a_R C_e^{\,n}}$
Sips	$q_e = \frac{q_m k_S C_e^{\,1/n}}{1+k_S C_e^{\,1/n}}$

Note: q_e and C_e denote the amount of dye adsorbed and the dye concentration at equilibrium, respectively, maximum adsorption capacity of the adsorbent is indicated by q_m, the isotherm constants of Langmuir, Freundlich, and Sips are by k_L, k_F, and k_S, isotherm constants of Temkin by k_T and b_T while the Redlich–Peterson isotherm constants by k_R and a_R, the empirical parameter related to adsorption intensity by n, mean free energy by β, gas constant and absolute temperature by R and T, respectively.

Table 2
Isotherm parameters and errors at different temperature

Model	298 K	313 K	323 K	333 K	343 K
Langmuir					
q_{max} (mmol g^{-1})	0.28	0.30	0.32	0.32	0.33
q_{max} (mg g^{-1})	131.36	140.47	146.24	148.90	154.43
K_L (L $mmol^{-1}$)	0.02	0.02	0.03	0.01	0.01
R^2	0.9732	0.9930	0.9955	0.9938	0.9643
ARE	20.24	7.39	15.65	7.68	12.26
HYBRID	0.68	0.27	0.91	0.16	0.39
EABS	0.38	0.17	0.493	0.13	0.31
MPSD	29.57	14.67	21.10	14.43	16.74
Freundlich					
K_F ($mmol^{1-1/n}$ $L^{1/n}$ g^{-1})	0.03	0.02	0.05	0.01	0.02
n	3.00	2.21	3.85	1.90	2.10
R^2	0.9837	0.9124	0.9258	0.9612	0.9401
ARE	8.59	14.69	11.00	13.73	13.06
HYBRID	0.14	0.75	0.31	0.55	0.47
EABS	0.17	0.42	0.2461	0.35	0.31
MPSD	15.96	21.22	18.35	19.38	18.84
Temkin					
K_T (L $mmol^{-1}$)	0.57	0.33	0.92	0.18	0.34
b_T (KJ mol^{-1})	58.50	46.71	62.50	40.75	45.06
R^2	0.9580	0.9760	0.9756	0.9830	0.9600
ARE	11.75	8.08	6.97	10.78	10.27
HYBRID	0.26	0.16	0.11	0.20	0.22
EABS	0.28	0.17	0.1668	0.14	0.23
MPSD	15.63	12.93	18.24	19.18	14.87
Dubinin–Radushkevich					
q_{max} (mmol g^{-1})	0.18	0.25	0.23	0.25	0.26
q_{max} (mg g^{-1})	85.32	117.36	108.15	116.02	121.89
B (J mol^{-1})	5.19E-07	1.08E-06	7.33E-07	1.34E-06	9.91E-07
E (kJ mol^{-1})	981.41	681.24	825.73	609.96	710.15
R^2	0.8927	0.9606	0.9616	0.9012	0.9431
ARE	94.41	85.36	58.13	130.21	123.21
HYBRID	11.20	16.14	8.90	27.10	24.43
EABS	1.42	1.02	0.7797	1.17	1.23
MPSD	166.50	178.02	116.07	258.12	254.33
Redlich–Peterson					
K_R (L mg^{-1})	0.06	0.01	0.01	0.05	0.01
A	0.68	0.87	0.98	0.52	0.84
a_R(L mg^{-1})	1.75	0.07	0.06	3.18	0.07
R^2	0.9905	0.9951	0.9960	0.9488	0.9749
ARE	7.69	7.29	3.75	13.38	8.04
HYBRID	0.12	0.20	0.08	0.43	0.22
EABS	0.17	0.16	0.1054	0.29	0.22
MPSD	12.95	13.63	6.61	19.49	11.74
Sips					
q_{max} (mmol g^{-1})	0.55	0.35	0.29	0.38	0.45
q_{max} (mg g^{-1})	254.93	162.23	134.42	176.13	208.58
K_S (L $mmol^{-1}$)	0.04	0.04	0.08	0.02	0.02
n	2.15	1.35	1.48	1.30	1.40
R^2	0.9743	0.9619	0.9618	0.9841	0.9709
ARE	7.62	7.64	5.64	9.14	9.77
HYBRID	0.14	0.22	0.1	0.17	0.33
EABS	0.17	0.17	0.143	0.12	0.26
MPSD	13.31	14.25	8.26	17.64	14.86

belong to the three-parameter isotherm models. The good fitting of Sips and R–P models to the adsorption data may be related to their higher degree of freedom, as Sips model is a combination of the Langmuir and Freundlich models which assumes mono- and multilayer adsorption of adsorbates onto the adsorbent's surface. Among Sips and R–P models, the latter gave the highest coefficient of determination, R^2, close to unity with lowest error values. However, based on the Sips isotherm model, the maximum adsorption capacity (q_{max}) of TL is estimated to be 254.9 mg g^{-1}, which is very high compared with those of many untreated and treated adsorbents, as shown in Table 3. For example, modified carbon nanotube and activated carbon that have been loaded with different nanoparticles all gave q_{max} lower than TL. Thus TL can be considered a very good adsorbent for the removal of MG and has a great potential to be used in real life wastewater treatment given its simple and easy preparation, without any elaborate and complicated treatment, where only heating in an oven was required.

3.5. Thermodynamic quantities

Thermodynamic quantities provide vital information about the adsorption process of MG on TL leaves. In this study, the adsorption of MG was found to be endothermic in nature as shown by the positive $\Delta H°$ value (4.14 kJ mol^{-1}). The increase in negative $\Delta G°$ values with increasing temperature indicates the spontaneity of the adsorption process, where temperature 298, 313, 323, 333, and 343 K resulted in –4.18, –4.88, –4.89, –5.27, and –5.50 kJ mol^{-1}, respectively. The $\Delta G°$ values of the adsorption are less than –20 kJ mol^{-1}, implying physisorption where electrostatic interactions are involved between the cationic dyes and the active sites, rather than chemisorption. Positive $\Delta S°$ value (28.2 J mol^{-1} K^{-1}) suggests that during the adsorption process, there is an increase in the randomness at the adsorbent–dye solution interface.

Table 3
Comparison of q_{max} between different adsorbents

Adsorbent	q_{max} (mg g^{-1})	Reference
Artocarpus odoratissimus leaf	131.4 (Langmuir) 254.9 (Sips)	This work
Artocarpus altilis skin	55.2	[51]
Artocarpus camansi (Breadnut) peel	180.0	[52]
NaOH-treated *Artocarpus camansi* (Breadnut) peel	353.0	[52]
Walnut shell	90.8	[62]
Azolla pinnata	87.0	[63]
H_3PO_4-treated *Azolla pinnata*	292.1	[63]
NaOH-treated *Azolla pinnata*	109.6	[63]
Casuarina equisetifolia	77.6	[64]
Modified sphagnum peat	122.0	[65]
Daucus carota stem	43.4	[66]
Daucus carota leaf	52.6	[66]
Poly(methacrylic acid) modified sugarcane bagasse	103.2	[67]

3.6. Kinetics at room temperature

Kinetics of the adsorption of MG onto TL was investigated using two different MG concentrations, that is, 100 and 500 mg L^{-1} and are shown in Fig. 5(A), where it can be observed that the ANN data agreed well with the experimental data. The kinetics mechanism was evaluated by fitting the adsorption data with the pseudo-first-order [68] and pseudo-second-order [69] reaction kinetics, as given by Eqs. (5) and (6), respectively:

$$\log\left(q_e - q_t\right) = \log\left(q_e\right) - \frac{t}{2.303}k_1 \tag{5}$$

$$\frac{t}{qt} = \frac{q}{k_2 {q_e}^2} + \frac{t}{q_e} \tag{6}$$

Here, the amount of dye adsorbed is denoted by q_t (mg g^{-1}), the pseudo-first-order and pseudo-second-order rate constants are represented by k_1 (min^{-1}) and k_2 (g mg^{-1} min^{-1}), respectively, and contact time is denoted by t (min).

From Figs. 5(B)–(E) and Table 4, it is clear that the pseudo-second-order reaction kinetics is better to fit the adsorption data, giving very high R^2 values close to unity. The calculated and experimental adsorption capacity ($q_{e,cal}$ and $q_{e,exp}$) further confirmed that the kinetics mechanism for the adsorption of MG onto TL is pseudo-second order. It can also be observed from Table 4 that as the dye concentration increases, the rate constant (k_2) decreases. This is in line with the pseudo-second-order kinetics where reported that the time required for equilibrium increases with adsorbate concentration [70].

In order to understand the diffusion mechanism involved, the Weber–Morris intraparticle diffusion model [71] ($q_t = k_3 t^{1/2} + c$, where k_3 (mg g^{-1} $min^{-1/2}$) is the intraparticle diffusion rate constant) was used to fit the adsorption data. In general, diffusion can be divided into three phases, which are the fast external diffusion, the intraparticle diffusion, and the equilibrium. The Weber–Morris intraparticle diffusion plot, as shown in Fig. 5(D), displayed multi-linearity behaviour. The fast external diffusion is usually completed within 5 min and it is not observed in the Weber–Morris intraparticle diffusion plot. This unobservable fast external diffusion has been reported in the adsorption of MG using *Azolla pinnata* as adsorbent [63]. The first linear region in Fig. 5(D) represents the intraparticle diffusion phase while the second linear region represents the slow equilibrium phase. According to the intraparticle diffusion model, if the plot passes through the origin, then the intraparticle diffusion phase is the rate-limiting. However, as seen in Table 5, the intercepts of the plots (denoted as *C*) are non-zero and these indicated that intraparticle diffusion of MG onto TL is not rate-limiting.

In addition, we have applied the Boyd intraparticle diffusion model [72] by plotting B_t as a function of t, according to $B_t = -0.4977 - \ln(1-F)$, where B_t is mathematical function of F, and $F = q_t/q_e$. The Boyd plot is shown in Fig. 5(C). According to the Boyd model, if the intercept of the Boyd plot is non-zero, the diffusion process is controlled by film diffusion, otherwise it is controlled by particle diffusion. Particle diffusion is referred to the adsorbates transfer onto the pores of the

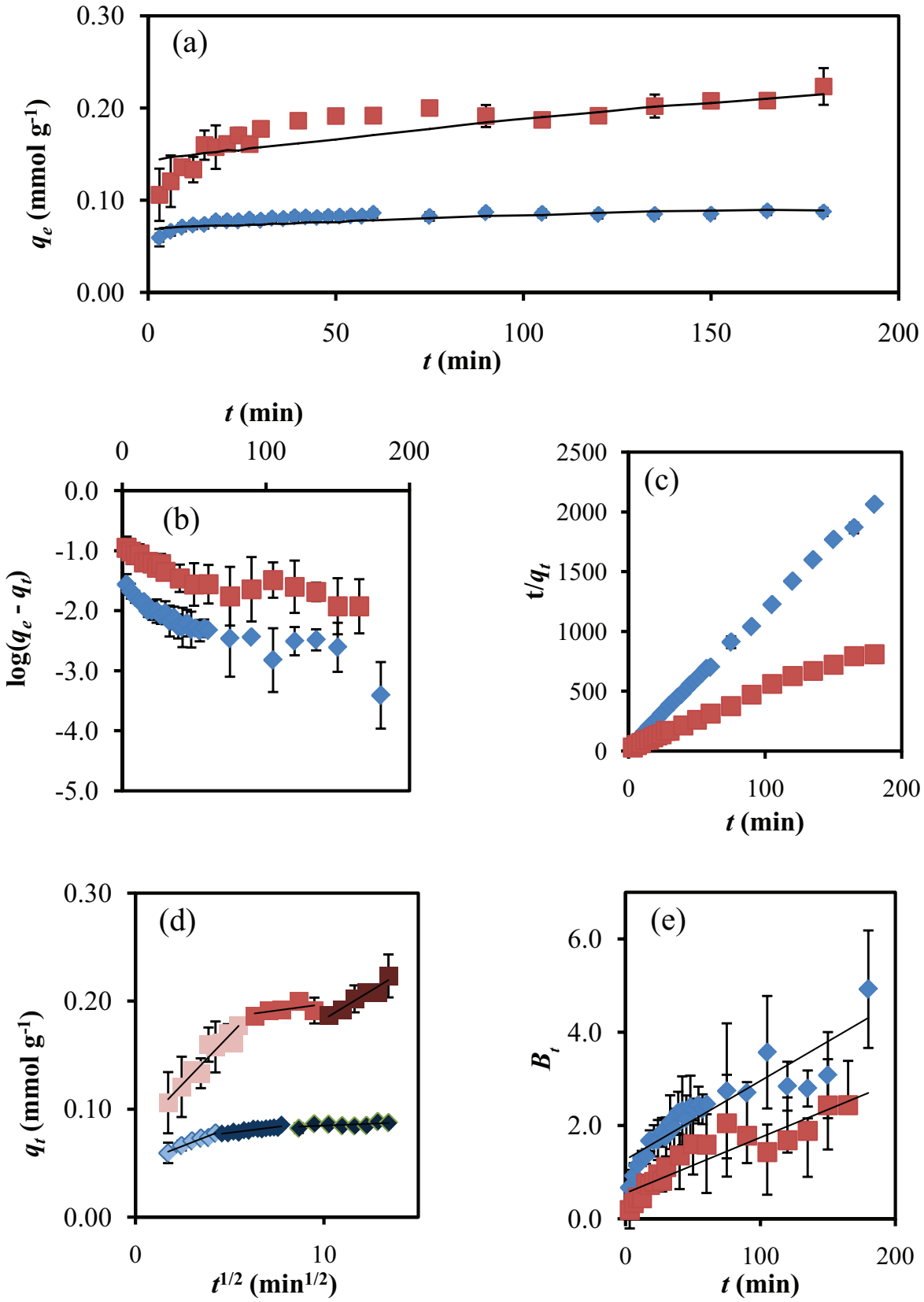

Fig. 5. (A) The adsorption of 100 mg L^{-1} (♦) and 500 mg L^{-1} (■) of MG onto TL with ANN data (—). The experimental data of kinetics were plotted using different kinetic models such as (B) pseudo-first order, (C) pseudo-second order, (D) intraparticle diffusion, and (E) Boyd using two concentration of MG, 100 mg L^{-1} (♦) and 500 mg L^{-1} (■).

Table 4
Parameters of pseudo-first-order and pseudo-second-order kinetic models

Concentration of MG (mg L^{-1})	Pseudo-first-order model			Pseudo-second-order model			q_{exp} (mmolg^{-1})
	k_1 (min^{-1})	q_{calc} (mmolg^{-1})	R^2	k_2 (gmmol^{-1} min^{-1})	q_{calc} (mmolg^{-1})	R^2	
100	0.017	0.015	0.827	3.91	0.088	0.999	0.093
500	0.012	0.078	0.827	0.65	0.216	0.994	0.229

Table 5
Parameters of kinetic diffusion models

Concentration of MG (mg L^{-1})	Intraparticle diffusion			Boyd	
	C (mg g^{-1})	k_i (mg $min^{1/2}$ g^{-1})	R^2	C	R^2
100	0.05	0.007	0.968	1.27	0.827
500	0.08	0.028	0.925	0.55	0.827

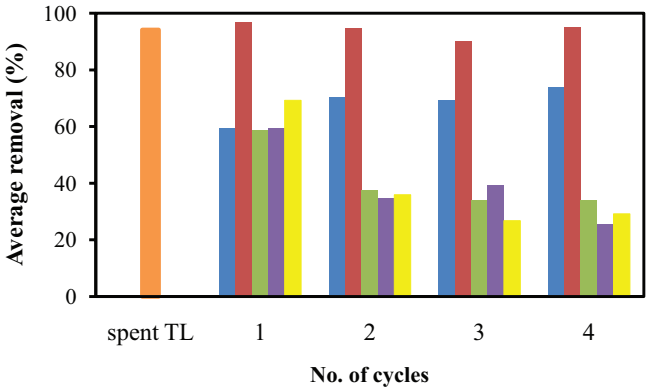

Fig. 6. Regeneration of spent TL (■) using 100 mg L^{-1} MG for four cycles using acid (■), base (■), water by rinsing (■), water by shaking (■) along with control (■).

adsorbent, while film diffusion means adsorbates transfer to the external surface of the adsorbent. As summarized in Table 5, all the intercepts are non-zero, indicating that the diffusion process is controlled by the film diffusion.

3.7. Regeneration of spent TL adsorbents

Spent adsorbents can carry several problems since some of them can be flammable, while the others may produce toxic substances. Thus, most of the spent adsorbents are considered hazardous and have to be incinerated. Recent attention has turned to regeneration of the spent adsorbents. The ability to regenerate and reuse a spent adsorbent adds value to the adsorbent. In this study, regeneration and reuse of the spent TL adsorbent were investigated. For this purpose, four different treatment methods of regeneration were implied, namely the spent TL adsorbent was rinsed with acid, base, water, and distilled water, and it was reused to remove MG. In Fig. 6 we showed dye removal by spent TL against the number of adsorption–desorption cycle. It is clearly observed that washing or quick rinsing the spent adsorbent with distilled water showed gradual degradation of removal efficiency, similarly to that of the spent TL adsorbent without treatment. The efficiency of MG removal decreased drastically to approximately 70% at the fourth cycle. Notably, acid treatment reduced its adsorption by 20% at the fourth cycle, while the spent TL adsorbent was well regenerated upon treatment with NaOH where the spent TL adsorbent was able to maintain its adsorption towards MG throughout the four cycles.

4. Conclusions

In this study we have investigated the potential of adsorbent from *Artocarpus odoratissimus* leaves for the removal of hazardous MG dye from aqueous solution. The adsorption process was well described by Sips and Redlich–Peterson isotherm models. The Sips model predicts the maximum adsorption capacity as high as 254.93 mg g^{-1}. The kinetics behaviour of the adsorption process is most likely a pseudo-second order and the diffusion models suggest that intraparticle diffusion may be controlled by film diffusion. The spent TL adsorbent can be well regenerated and reused upon treatment with strong basic solution. This study also showed that the ANN model was able to accurately predict some of the experimental data.

Acknowledgements

The authors are grateful to the Government of Negara Brunei Darussalam, the Universiti Brunei Darussalam, CAMES and Department of Biological Sciences for their continual support.

References

[1] M. Chiou, P. Ho, H. Li, Adsorption of anionic dyes in acid solutions using chemically cross-linked chitosan beads, Dyes Pigm., 60 (2004) 69–84.
[2] L. Karimi, S. Zohoori, M.E. Yazdanshenas, Photocatalytic degradation of azo dyes in aqueous solutions under UV irradiation using nano-strontium titanate as the nanophotocatalyst, J. Saudi Chem. Soc., 18 (2014) 581–588.
[3] R. Saravanan, V.K. Gupta, E. Mosquera, F. Gracia, V. Narayanan, A. Stephen, Visible light induced degradation of methyl orange using β-Ag 0.333 V_2O_5 nanorod catalysts by facile thermal decomposition method, J. Saudi Chem. Soc., 19 (2015) 521–527.
[4] Y.M. Slokar, A.M. Le Marechal, Methods of decoloration of textile wastewaters, Dyes Pigm., 37 (1998) 335–356.
[5] Y. Sun, H. Hu, C.Z. Shi, Z. Yang, F. Tang, Changes in the components and biotoxicity of dissolved organic matter in a municipal wastewater reclamation reverse osmosis system, Environ. Technol., 37 (2016) 2149–2156.
[6] G. Crini, Non-conventional low-cost adsorbents for dye removal: a review, Bioresour. Technol., 97 (2006) 1061–1085.
[7] M. Rafatullah, O. Sulaiman, R. Hashim, A. Ahmad, Adsorption of methylene blue on low-cost adsorbents: a review, J. Hazard. Mater., 177 (2010) 70–80.
[8] A. Demirbas, Heavy metal adsorption onto agro-based waste materials: a review, J. Hazard. Mater., 157 (2008) 220–229.

[9] W.S. Wan Ngah, L.C. Teong, M.A.K.M. Hanafiah, Adsorption of dyes and heavy metal ions by chitosan composites: a review, Carbohydr. Polym., 83 (2011) 1446–1456.
[10] G.M. Gadd, Biosorption: critical review of scientific rationale, environmental importance and significance for pollution treatment, J. Chem. Technol. Biotechnol., 84 (2009) 13–28.
[11] G. Xiao, Z. Li, T.L. Saleman, E.F. May, Adsorption equilibria and kinetics of CH_4 and N_2 on commercial zeolites and carbons, Adsorption, 23 (2017) 131–147.
[12] R.S.P. Couto, A.F. Oliveira, A.W.S. Guarino, D.V. Perez, M.R.C. Marques, Removal of ammonia nitrogen from distilled old landfill leachate by adsorption on raw and modified aluminosilicate, Environ. Technol., 38 (2017) 816–826.
[13] T.A. Saleh, A. Sarı, M. Tuzen, Optimization of parameters with experimental design for the adsorption of mercury using polyethylenimine modified-activated carbon, J. Environ. Chem. Eng., 5 (2017) 1079–1088.
[14] M.H. El-Naas, M.A. Alhaija, S. Al-Zuhair, Evaluation of an activated carbon packed bed for the adsorption of phenols from petroleum refinery wastewater, Environ. Sci. Pollut. Res., 24 (2017) 7511–7520.
[15] A. Barhoumi, S. Ncib, W. Bouguerra, B. Hamrouni, E. Elaloui, Combining adsorption on activated carbon with electrocoagulation process for copper removal from used water, Desal. Wat. Treat., 83 (2017) 212–221.
[16] H. Tahir, M. Sultan, N. Akhtar, U. Hameed, T. Abid, Application of natural and modified sugar cane bagasse for the removal of dye from aqueous solution, J. Saudi Chem. Soc., 20 (2016) 115–121.
[17] U.J. Etim, S.A. Umoren, U.M. Eduok, Coconut coir dust as a low cost adsorbent for the removal of cationic dye from aqueous solution, J. Saudi Chem. Soc., 20 (2016) 67–76.
[18] A.K. Shah, Z.M. Ali, A.J. Laghari, S.F.A. Shah, Utilization of fly ash as low-cost adsorbent for the treatment of industrial dyes effluents - a comparative study, Res. Rev. J. Eng. Technol., 2 (2013) 1–10.
[19] L.B.L. Lim, N. Priyantha, C.M. Chan, D. Matassan, H.I. Chieng, M.R.R. Kooh, Adsorption behavior of methyl violet 2B using duckweed: equilibrium and kinetics studies, Arab. J. Sci. Eng., 39 (2014) 6757–6765.
[20] M.R.R. Kooh, M.K. Dahri, L.B.L. Lim, L.H. Lim, Batch adsorption studies on the removal of acid blue 25 from aqueous solution using *Azolla pinnata* and soya bean waste, Arab. J. Sci. Eng., 41 (2016) 2453–2464.
[21] L.B.L. Lim, N. Priyantha, C.M. Chan, D. Matassan, H.I. Chieng, M.R.R. Kooh, Investigation of the sorption characteristics of water lettuce (WL) as a potential low-cost biosorbent for the removal of methyl violet 2B, Desal. Wat. Treat., 57 (2016) 8319–8329.
[22] L.B.L. Lim, N. Priyantha, N.H. Mohd Mansor, *Artocarpus altilis* (breadfruit) skin as a potential low-cost biosorbent for the removal of crystal violet dye: equilibrium, thermodynamics and kinetics studies, Environ. Earth Sci., 73 (2015) 3239–3247.
[23] H.I. Chieng, N. Priyantha, L.B.L. Lim, Effective adsorption of toxic brilliant green from aqueous solution using peat of Brunei Darussalam: isotherms, thermodynamics, kinetics and regeneration studies, RSC Adv., 5 (2015) 34603–34615.
[24] L. Sepúlveda, K. Fernández, E. Contreras, C. Palma, Adsorption of dyes using peat: equilibrium and kinetic studies, Environ. Technol., 25 (2004) 987–996.
[25] T. Zehra, N. Priyantha, L.B.L. Lim, E. Iqbal, Sorption characteristics of peat of Brunei Darussalam V: removal of congo red dye from aqueous solution by peat, Desal. Wat. Treat., 54 (2015) 2592–2600.
[26] S.M. Al-Rashed, A.A. Al-Gaid, Kinetic and thermodynamic studies on the adsorption behavior of Rhodamine B dye on Duolite C-20 resin, J. Saudi Chem. Soc., 16 (2012) 209–215.
[27] N.F. Ali, R.S.R. El-Mohamedy, Microbial decolourization of textile waste water, J. Saudi Chem. Soc., 16 (2012) 117–123.
[28] G. Resmi, S.G. Thampi, S. Chandrakaran, Removal of lead from wastewater by adsorption using acid-activated clay, Environ. Technol., 33 (2012) 291–297.
[29] M.P. Elizalde-González, A.A. Peláez-cid, Removal of textile dyes from aqueous solutions by adsorption on biodegradable wastes, Environ. Technol., 24 (2003) 821–829.
[30] S. Çoruh, F. Geyikçi, O. Nuri Ergun, Adsorption of basic dye from wastewater using raw and activated red mud, Environ. Technol., 32 (2011) 1183–1193.
[31] A. Bhatnagar, M. Sillanpaa, Utilization of agro-industrial and municipal waste materials as potential adsorbents for water treatment - a review, Chem. Eng. J., 157 (2010) 277–296.
[32] A. Bhatnagar, A.K. Minocha, Conventional and non-conventional adsorbents for removal of pollutants from water – a review, Ind. J. Chem. Technol., 13 (2006) 203–217.
[33] S.S. Baboo, I.K. Shereef, An efficient weather forecasting system using artificial neural network, Int. J. Environ. Sci. Dev., 1 (2010) 321–326.
[34] M.P. Naeini, H. Taremian, H.B. Hashemi, Stock Market Value Prediction Using Neural Networks, in: Computer Information Systems and Industrial Management Applications (CISIM), International Conference on IEEE, 2010, pp. 132–136.
[35] C.A.O. Nascimento, R. Giudici, R. Guardani, Neural network based approach for optimization of industrial chemical processes, Comput. Chem. Eng., 24 (2000) 2303–2314.
[36] H.M. Nagy, K.A.N.D. Watanabe, M. Hirano, Prediction of sediment load concentration in rivers using artificial neural network model, J. Hydraul. Eng., 128 (2002) 588–595.
[37] A.M. Ghaedi, A. Vafaei, Applications of artificial neural networks for adsorption removal of dyes from aqueous solution: a review, Adv. Colloid Interface Sci., 245 (2017) 20–39.
[38] M.R.R. Kooh, L.B.L. Lim, L.H. Lim, O.A. Malik, Phytoextraction potential of water fern (*Azolla pinnata*) in the removal of a hazardous dye, methyl violet 2B: artificial neural network modelling, Int. J. Phytorem., (2017) doi:10.1080/15226514.2017.1365337.
[39] M.R.R. Kooh, M.K. Dahri, L.B.L. Lim, L.H. Lim, O.A. Malik, Batch adsorption studies of the removal of methyl violet 2B by soya bean waste: isotherm, kinetics and artificial neural network modelling, Environ. Earth Sci., 75 (2016) 783.
[40] H. Serudin, D.S. Haji Tinggal, Tarap (*Artocarpus odoratissimus*): potential tropical fruit for food product opportunities, Front. Tropical Fruit Res., 321 (1991) 106–111.
[41] M. Uddin, M. Rukanuzzaman, M. Khan, M. Rahman, M. Islam, Jackfruit (*Artocarpus heterophyllus*) leaf powder: an effective adsorbent for removal of methylene blue from aqueous solutions, Ind. J. Chem. Technol., 16 (2009) 142–149.
[42] K. Ojha, V.K. Bulasara, Adsorption characteristics of jackfruit leaf powder for the removal of Amido black 10B dye, Environ. Prog. Sustain. Energy, 34 (2015) 461–470.
[43] L.B.L. Lim, N. Priyantha, C. Hei Ing, M. Khairud Dahri, D.T.B. Tennakoon, T. Zehra, M. Suklueng, *Artocarpus odoratissimus* skin as a potential low-cost biosorbent for the removal of methylene blue and methyl violet 2B, Desal. Wat. Treat., 53 (2015) 964–975.
[44] M.K. Dahri, M.R.R. Kooh, L.B.L. Lim, *Artocarpus odoratissimus* (Tarap) core as an adsorbent for the removal of crystal violet dye from aqueous solution, J. Mater. Environ. Sci., 8 (2017) 3706–3717.
[45] L.B.L. Lim, N. Priyantha, T. Zehra, C.W. Then, C.M. Chan, Adsorption of crystal violet dye from aqueous solution onto chemically treated *Artocarpus odoratissimus* skin: equilibrium, thermodynamics, and kinetics studies, Desal. Wat. Treat., 57 (2016) 10246–10260.
[46] L.B.L. Lim, N. Priyantha, X.Y. Fang, N.A.H.M. Zaidi, *Artocarpus odoratissimus* peel as a potential adsorbent in environmental remediation to remove toxic Rhodamine B dye, J. Mater. Environ. Sci., 8 (2017) 494–502.
[47] L.B.L. Lim, N. Priyantha, N.A.H.M. Zaidi, U.A.N. Jamil, H.I. Chieng, T. Zehra, A. Liyandeniya, Chemical modification of *Artocarpus odoratissimus* skin for enhancement of their adsorption capacities toward toxic malachite green dye, J. Mater. Environ. Sci., 7 (2016) 3211–3224.
[48] M.K. Dahri, L.B.L. Lim, M.R.R. Kooh, C.M. Chan, Adsorption of brilliant green from aqueous solution by unmodified and chemically modified Tarap (*Artocarpus odoratissimus*) peel, Int. J. Environ. Sci. Technol., 14 (2017) 2683–2694.

[49] F.J. Green. The Sigma-Aldrich Handbook of Stains, Dyes and Indicators, Aldrich Chemical Co., 1990.
[50] M. Hall, E. Frank, G. Holmes, B. Pfahringer, P Reutemann, I.H. Witten, The WEKA data mining software: an update, ACM SIGKDD Explor., 11 (2009) 10–18.
[51] L.B.L. Lim, N. Priyantha, N.H. Mohd Mansor, Utilizing *Artocarpus altilis* (breadfruit) skin for the removal of malachite green: isotherm, kinetics, regeneration, and column studies, Desal. Wat. Treat., 57 (2016) 16601–16610.
[52] H.I. Chieng, L.B.L. Lim, N. Priyantha, Enhancing adsorption capacity of toxic malachite green dye through chemically modified breadnut peel: equilibrium, thermodynamics, kinetics and regeneration studies, Environ. Technol., 36 (2015) 86–97.
[53] M.R.R. Kooh, L.B.L. Lim, M.K. Dahri, L.H. Lim, J.M.R.S. Bandara, *Azolla pinnata*: an efficient low cost material for removal of methyl violet 2B by using adsorption method, Waste Biomass Valorization, 6 (2015) 547–559.
[54] M.K. Dahri, L.B.L. Lim, C.C. Mei, Cempedak durian as a potential biosorbent for the removal of Brilliant Green dye from aqueous solution: equilibrium, thermodynamics and kinetics studies, Environ. Monit. Assess., 187 (2015) 546.
[55] L.B.L. Lim, N. Priyantha, D.T.B. Tennakoon, H.I. Chieng, M.K. Dahri, M. Suklueng, Breadnut peel as a highly effective low-cost biosorbent for methylene blue: equilibrium, thermodynamic and kinetic studies, Arab. J. Chem., 10 (2017) S3216–S3228.
[56] I. Langmuir, The constitution and fundamental properties of solids and liquids, J. Franklin Inst., 183 (1917) 102–105.
[57] H.M.F. Freundlich, Over the adsorption in the solution, J. Phys. Chem., 57 (1906) 384–470.
[58] M. Temkin, V. Pyzhev, Kinetics of ammonia synthesis on promoted iron catalysts, Acta Physiochim. URSS, 12 (1940) 217–222.
[59] M.M. Dubinin, L.V. Radushkevich, The equation of the characteristic curve of activated charcoal, Proc. Acad. Sci. Phys. Chem. Sec., 55 (1947) 331–337.
[60] O. Redlich, D.L. Peterson, A useful adsorption isotherm, J. Phys. Chem., 63 (1959) 1024–1024.
[61] R. Sips, On the structure of a catalyst surface, J. Chem. Phys., 16 (1948) 490–495.
[62] M.K. Dahri, M.R.R. Kooh, L.B.L. Lim, Water remediation using low cost adsorbent walnut shell for removal of malachite green: equilibrium, kinetics, thermodynamic and regeneration studies, J. Environ. Chem. Eng., 2 (2014) 1434–1444.
[63] M.R.R. Kooh, L.B.L. Lim, L.H. Lim, J.M.R.S. Bandara, Batch adsorption studies on the removal of malachite green from water by chemically modified *Azolla pinnata*, Desal. Wat. Treat., 57 (2016) 14632–14646.
[64] M.K. Dahri, M.R.R. Kooh, L.B.L. Lim, Application of *Casuarina equisetifolia* needle for the removal of methylene blue and malachite green dyes from aqueous solution, Alexandria Eng. J., 54 (2015) 1253–1263.
[65] F. Hemmati, R. Norouzbeigi, F. Sarbisheh, H. Shayesteh, Malachite green removal using modified sphagnum peat moss as a low-cost biosorbent: kinetic, equilibrium and thermodynamic studies, J. Taiwan Inst. Chem. Eng., 58 (2016) 482–489.
[66] A.K. Kushwaha, N. Gupta, M.C. Chattopadhyaya, Removal of cationic methylene blue and malachite green dyes from aqueous solution by waste materials of *Daucus carota*, J. Saudi Chem. Soc., 18 (2014) 200–207.
[67] Y. Xing, G. Wang, Poly (methacrylic acid)-modified sugarcane bagasse for enhanced adsorption of cationic dye, Environ. Technol., 30 (2009) 611–619.
[68] S. Lagergren, About the theory of so called adsorption of soluble substances, K. Sven. Vetensk.akad. Handl., 24 (1898) 1–39.
[69] Y.S. Ho, G. McKay, Sorption of dye from aqueous solution by peat, Chem. Eng. J., 70 (1998) 115–124.
[70] W. Plazinski, W. Rudzinski, A. Plazinska, Theoretical models of sorption kinetics including a surface reaction mechanism: a review, Adv. Colloid Interface Sci., 152 (2009) 2–13.
[71] W.J. Weber, J.C. Morris, Kinetics of adsorption on carbon from solution, J. Sanit. Eng. Div. 89 (1963) 31–60.
[72] G.E. Boyd, A.W. Adamson, L.S. Myers Jr., The exchange adsorption of ions from aqueous solutions by organic zeolites II Kinetics, J. Am. Chem. Soc., 69 (1947) 2836–2848.